

Frequency-Switching Sparse Arrays

Yimin D. Zhang and Md. Waqeeb T. S. Chowdhury

Department of Electrical and Computer Engineering, Temple University, Philadelphia, PA 19122, USA

Abstract—In this paper, we propose high-resolution target direction-of-arrival (DOA) estimation using frequency-switching sparse arrays which implement multi-frequency sparse arrays in a low-complexity manner. Unlike multi-frequency sparse arrays which require processing of wideband signals comprising multiple frequency components, the proposed frequency-switching sparse arrays only need to process a single-frequency component at any time instant, thereby eliminating such hurdles and significantly reducing the system complexity. A frequency-switching sparse array achieves the same number of degrees-of-freedom as a multi-frequency counterpart with comparable DOA estimation performance. Numerical results on the DOA estimation performance and Cramer-Rao bounds are provided to illustrate the effectiveness of the proposed frequency-switching sparse arrays.

Index Terms—Sparse array, direction-of-arrival estimation, frequency diversity, frequency-switching, group sparsity

I. INTRODUCTION

Direction-of-arrival (DOA) estimation of targets using sparse arrays has attracted great interests over the last few decades due to their capability to achieve a higher number of degrees-of-freedom (DOFs) compared to the uniform array counterparts. A well-designed N -element sparse linear array can achieve $\mathcal{O}(N^2)$ DOFs [1, 2]. Various systematical sparse array structures, such as the coprime array [3], the nested array [4], and the maximum inter-element spacing constraint (MISC) array [5], have been developed that have closed-form expressions of their sparse sensor positions, thus allowing convenient design and analysis of their lags and achievable DOFs. Inspired by these array configurations, a number of systematical sparse array design schemes have been developed [6–13].

One such novel approach of sparse array design is by taking advantages of the property that the array manifold is frequency-dependent. This property enables construction of a virtual coprime array using a single uniform linear array (ULA) with two frequencies [14]. Such array design extends the coprime array concept developed in the spatial domain using two physical subarrays to a joint spatio-spectral domain with a single physical subarray. As such, it achieves far more DOFs than the number of physical sensors, offering a significant flexibility in sparse array design to meet both DOF and system complexity requirements. An analysis of the Cramer-Rao bound (CRB) of the virtual coprime array is considered in [15] for a ULA using two coprime frequencies. The extension to multi-frequency case along with an analysis of the achievable DOFs are studied in [16–19]. In addition, multi-frequency sparse array structures are designed in [20] such that the resulting difference coarrays are free of redundant lags, thus achieving the highest possible number of DOFs for a given number of physical sensors. Sensor interpolation techniques are used in [21, 22] so that missing virtual elements can be filled for enhanced DOA estimation. Rational multi-frequency sparse arrays are considered in [23, 24] to facilitate flexible design of multi-frequency sparse arrays.

It should be noted that, although multi-frequency sparse array designs are lucrative in terms of the increased number of DOFs and higher design flexibility, the frequency span of multi-frequency signals render a high bandwidth at the receiver output, thus requiring

more complicated receiver processing which is undesirable and may even be infeasible for some applications.

This paper develops the concept of frequency-switching sparse array which aims to achieve the same frequency diversity as multi-frequency sparse arrays but with a low complexity. By switching between the available frequencies within the coherent processing interval (CPI), frequency-switching sparse arrays only handle a single-frequency component at any time instance, thus the receiver processing remains narrowband. The signals received in the frequency-switching sparse array can be formulated in a similar manner as that of the multi-frequency sparse array, and thus processed using same methods, such as the group-LASSO [26, 27], that account for the phase uncertainty of the received signals corresponding to different carrier frequencies.

Compared to multi-frequency sparse arrays, the frequency-switching scheme benefits from a higher signal power and, at the same time, suffers from reduced number of data samples. As such, the frequency-switching scheme achieves similar performance as the multi-frequency sparse arrays. Numerical results are provided to demonstrate their performance difference with respect to the input signal-to-noise ratio (SNR) and the number of data samples.

Notations: We use lower-case (upper-case) bold characters to denote vectors (matrices). In particular, \mathbf{I}_N denotes the $N \times N$ identity matrix. $(\cdot)^*$, $(\cdot)^T$, and $(\cdot)^H$ respectively represent the complex conjugate, transpose, and the Hermitian operations. $\mathbb{E}(\cdot)$ stands for statistical expectation, and $j = \sqrt{-1}$ stands for the unit imaginary number. $\|\cdot\|_2$ and $\|\cdot\|_{1,2}$ denote the l_2 norm and the mixed $l_{1,2}$ norm, respectively, and $|\cdot|$ represents the absolute value. Furthermore, \otimes and \cup respectively denote the Kronecker product and union operators. $\delta(i, j)$ is the Kronecker delta function which equals 1 when $i = j$ and 0 otherwise. Finally, $\mathbb{C}^{M \times N}$ denotes the $M \times N$ complex space.

II. MULTI-FREQUENCY SPARSE ARRAY

In this section, we review the array and signal models for multi-frequency sparse arrays and their covariance matrices [14, 17, 21].

A. Array Model

Consider I continuous-wave (CW) signals with carrier frequencies f_i , $i = 1, 2, \dots, I$, which are reflected from K far-field targets. Fig. 1(a) illustrates that the I frequencies are activated over the entire time, although their exact time occupancy depends on the duty cycles of the transmitted waveform being used. The reflected signals impinge on the receive array with N physical sensors, which can be either a uniform or a sparse linear array. Denote the locations of the physical array sensors as $\mathbb{P} = \{l_0, l_1, \dots, l_{N-1}\}d$, where $l_0 = 1$, and d denotes the unit inter-element spacing. It should be noted that the I frequencies of the CW signals are related by the following:

$$\frac{M_1}{f_1} = \frac{M_2}{f_2} = \dots = \frac{M_I}{f_I} = \frac{2d}{c}, \quad (1)$$

where c is the propagation velocity of electromagnetic waves in the free space. We assume that M_i , $i = 1, \dots, I$, take integer values such that the inter-element spacing $d = M_i \lambda_i / 2$ is an integer multiple of half-wavelength in the respective frequencies. The set of sensor

locations of the virtual array corresponding to the i th frequency is obtained as

$$\tilde{\mathbb{P}}_i = \{0, M_i l_1, M_i l_2, \dots, M_i l_{N-1}\} \lambda_i / 2. \quad (2)$$

As such, the virtual sensors associated with each frequency have different positions which are sparsely located on the half-wavelength grid. To obtain a high number of virtual sensors, these virtual sensor positions should be chosen distinctly.

Denote the integer coefficients of the virtual sensor positions with respect to half-wavelength at the respective frequency as

$$\mathbb{P}_i = \{0, M_i l_1, M_i l_2, \dots, M_i l_{N-1}\}. \quad (3)$$

For the entire multi-frequency sparse array, all the data corresponding to the I frequencies are observed and the total virtual array thus becomes

$$\mathbb{P}_v = \bigcup_{i=1}^I \mathbb{P}_i. \quad (4)$$

Fig. 2 shows an example of the virtual array where 5 physical sensors with two frequencies form a virtual array of 9 elements. Note that the element at position 0 is shared by the two virtual subarrays \mathbb{P}_1 and \mathbb{P}_2 obtained from both frequencies.

B. Signal Model

The radio-frequency (RF) signal vector corresponding to all I frequency components is expressed as

$$\tilde{\mathbf{x}}'(t) = \sum_{i=1}^I \tilde{\mathbf{y}}'_i(t) + \tilde{\mathbf{n}}'(t) = \sum_{i=1}^I \mathbf{A}_i \mathbf{s}'_i(t) e^{j2\pi f_i t} + \tilde{\mathbf{n}}'(t), \quad (5)$$

where $\tilde{\mathbf{y}}'_i(t)$ is the noise-free RF vector component corresponding to the i th frequency, $\mathbf{a}_i(\theta) = [1, e^{-j\pi M_i l_1 \sin(\theta)}, \dots, e^{-j\pi M_i l_{N-1} \sin(\theta)}]^T$ is the steering vector of the i th virtual array for signal arriving from θ , $\rho'_k{}^{(i)}(t)$ is the reflection coefficient of the k th target corresponding to the i th frequency, $\mathbf{s}_i(t) = [\rho'_1{}^{(i)}(t), \dots, \rho'_K{}^{(i)}(t)]^T$ is the complex magnitude of the signal of the i th frequency component, and $\tilde{\mathbf{n}}'_i(t) \sim \mathcal{CN}(\mathbf{0}, \sigma_n^2 \mathbf{I}_N)$ is the bandpass additive white Gaussian noise (AWGN). The manifold matrix of the i th virtual array is denoted as $\mathbf{A}_i = [\mathbf{a}_i(\theta_1), \mathbf{a}_i(\theta_2), \dots, \mathbf{a}_i(\theta_K)] \in \mathbb{C}^{N \times K}$. We used $(\cdot)'$ to denote the results for the multi-frequency sparse array where they differ to the frequency-switching counterparts to be described in Section III.

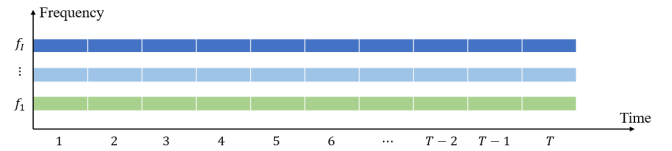
The complex magnitude $\rho'_k{}^{(i)}(t)$ is determined by the transmit signal power, path loss, and radar cross section (RCS) at the i th frequency, given as

$$\rho'_k{}^{(i)}(t) = \sqrt{P_i} \beta_k^{(i)} \sigma_k^{(i)}(t), \quad (6)$$

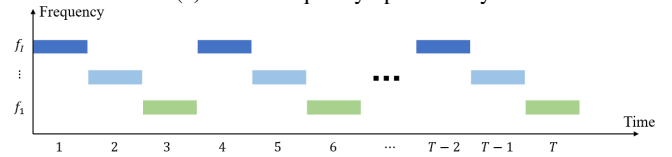
where P_i is the transmit power used for the i th frequency component, and the transmit power in all the I frequencies is subject to the total power constraint, i.e., $\sum_{i=1}^I P_i = P$. In addition, $\beta_k^{(i)} = \alpha \lambda_i / r_k^2$ is the path loss with r_k denoting the range of the k th target from the array and α is a constant determined by the sensor directional gains. In addition, $\sigma_k^{(i)}(t)$ is the RCS which is assumed to be independently time-varying over slow-time so that they are treated as uncorrelated. In case that the transmit power is equally distributed to the I frequencies, we have $P_i = P/I$ for $i = 1, \dots, I$.

Because $\tilde{\mathbf{x}}'(t)$ contains multiple frequency components, the analog-to-digital converter (ADC) would need to have a high bandwidth even as the RF signal is down-converted with respect to some signal carrier. When all the I frequency components are separately obtained in their baseband version, they are expressed as

$$\mathbf{x}'_i(t) = \mathbf{A}_i \mathbf{s}'_i(t) + \mathbf{n}'_i(t) = \sum_{k=1}^K \rho'_k{}^{(i)}(t) \mathbf{a}_i(\theta_k) + \mathbf{n}_i(t) \quad (7)$$



(a) Multi-frequency sparse array



(b) Frequency-switching sparse array

Fig. 1: Array configurations of multi-frequency and frequency-switching sparse arrays.

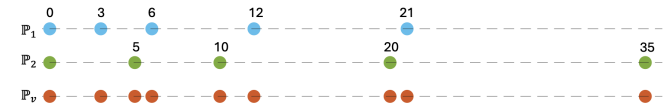


Fig. 2: Sensor location of the virtual arrays when $\mathbb{P} = \{0, 1, 2, 4, 7\}$, $M_1 = 3$ and $M_2 = 5$.

for $i = 1, \dots, I$, where $\mathbf{n}'_i(t)$ is the noise component at the i th frequency.

C. Covariance Matrices

The self-covariance matrix of the received data vector $\mathbf{x}_i(t)$ is obtained as

$$\mathbf{R}'_{ii} = \mathbb{E}[\mathbf{x}'_i(t) \mathbf{x}'_i{}^H(t)] = \mathbf{A}_i \mathbf{R}'_s{}^{(ii)} \mathbf{A}_i^H + \sigma_n^2 \mathbf{I}_N \quad (8)$$

for $i = 1, \dots, I$, where $\mathbf{R}'_s{}^{(ii)} = \mathbb{E}[\mathbf{s}'_i(t) \mathbf{s}'_i{}^H(t)]$ is the covariance matrix of the reflected signal vector for frequency f_i and is a diagonal matrix with real entries.

Similarly, the cross-covariance matrix between the received data vectors $\mathbf{x}'_i(t)$ and $\mathbf{x}'_j(t)$ is obtained as

$$\mathbf{R}'_{ij} = \mathbb{E}[\mathbf{x}'_i(t) \mathbf{x}'_j{}^H(t)] = \mathbf{A}_i \mathbf{R}'_s{}^{(ij)} \mathbf{A}_j^H \quad (9)$$

for $i \neq j$, where $\mathbf{R}'_s{}^{(ij)} = \mathbb{E}[\mathbf{s}'_i(t) \mathbf{s}'_j{}^H(t)]$ is the cross-covariance matrix of the reflected signal vectors for frequencies f_i and f_j . Matrix $\mathbf{R}'_s{}^{(ij)}$ is also diagonal but its diagonal elements generally take complex values because the signals corresponding to different frequencies experience diverse reflection coefficients as well as distinct propagation phase delays.

In practice, the exact covariance matrices are unavailable and are estimated from T data samples that are available within the CPI. The sample self- and cross-covariance matrices are respectively given as

$$\hat{\mathbf{R}}'_{ii} = \frac{1}{T} \sum_{t=1}^T \mathbf{x}'_i(t) \mathbf{x}'_i{}^H(t) \quad \text{and} \quad \hat{\mathbf{R}}'_{ij} = \frac{1}{T} \sum_{t=1}^T \mathbf{x}'_i(t) \mathbf{x}'_j{}^H(t). \quad (10)$$

III. FREQUENCY-SWITCHING SPARSE ARRAY MODEL

While multi-frequency sparse arrays enjoy a significant benefit in terms of a high number of DOFs and an extended aperture from its virtual arrays, the received signals containing multiple frequency components do not support narrowband signal processing as in conventional radar after pulse compression at the receiver. A wideband output comprising multiple frequency components at the

receiver would translate to wideband ADC and high-rate processing, thereby hindering the applicability to practical radar systems.

To address this issue, in this paper, we develop a frequency-switching version of the multi-frequency sparse array such that, instead of transmitting and processing multiple frequency components at the same time, different frequency components take a turn and only one frequency component is transmitted and processed at any time. For simplicity and without losing generality, we consider an equal division of the T available samples over the CPI into the I frequency components so that each frequency component would have T/I data samples. Depending on the way the frequency-switching signals are processed, different switching patterns may impact the estimation results of other parameters, such as the Doppler and range [28–30]. However, when the DOA estimation performance is concerned, only the number of data samples would be of interest.

The received RF signal vector at time t is expressed as

$$\tilde{\mathbf{x}}(t) = \tilde{\mathbf{x}}_i(t) = \sum_{k=1}^K \rho_k^{(i)}(t) \mathbf{a}_i(\theta_k) + \mathbf{n}_i(t) = \mathbf{A}_i \mathbf{s}_i(t) + \mathbf{n}_i(t). \quad (11)$$

This expression is similar to (5) with several important differences. First, at any time t , only one frequency component with $i \in \{1, \dots, I\}$ exists. Second, because all the transmit power will be dedicated to a single-frequency component at any time, the complex magnitude $\rho_k^{(i)}(t)$ is now changed to

$$\rho_k^{(i)}(t) = \sqrt{P} \beta_k^{(i)} \sigma_k^{(i)}(t). \quad (12)$$

On the other hand, the available number of snapshots T during a CPI is partitioned into I segments T_1, \dots, T_I for the I frequencies such that $\sum_{i=1}^I T_i = T$. In this paper, we assume equal-length partition with $T_i = T/I$.

Comparing (11) and (12) with (5) and (6), when the same total power is used and equally distributed in the multi-frequency sparse array scheme, the frequency-switching scheme benefits from the higher signal power by a factor of I while it suffers from the reduced number of data samples by the same factor of I .

IV. DOA ESTIMATION

A. Covariance Matrices

The self-covariance matrix of the received data vector $\mathbf{x}_i(t)$ is formulated as

$$\mathbf{R}_{ii} = \mathbb{E}[\mathbf{x}_i(t) \mathbf{x}_i^H(t)] = \mathbf{A}_i \mathbf{R}_s^{(ii)} \mathbf{A}_i^H + \sigma_n^2 \mathbf{I}_N \quad (13)$$

for $i = 1, \dots, I$, where covariance matrix $\mathbf{R}_s^{(ii)} = \mathbb{E}[\mathbf{s}_i(t) \mathbf{s}_i^H(t)]$ is diagonal with real entries. Note that, $\mathbf{R}_s^{(ii)} = (P/P_i) \mathbf{R}_s^{\prime(i)} = I \mathbf{R}_s^{\prime(i)}$ when the transmit power is equally distributed to all I frequencies in the multi-frequency sparse array.

For the cross-covariance matrix between two different frequency components, we need to consider the fact that these frequency components are transmitted and received at different time sample periods. Suppose that, for a data sample of the f_1 component sampled at t , the corresponding data sample of the f_i component is obtained at $t + \Delta t_i$, which introduces an additional phase term $e^{-j2\pi f_i \Delta t_i}$ compared to the signal if sampled at t . Because both f_i and Δt_i are known, this phase term can be compensated for so that the sampling timing difference does not affect the computation of the cross-covariance matrices.

The cross-covariance matrix between received data vectors $\mathbf{x}_i(t + \Delta t_i)$ and $\mathbf{x}_j(t + \Delta t_j)$ is expressed as

$$\mathbf{R}_{ij} = \mathbb{E}[\mathbf{x}_i(t + \Delta t_i) \mathbf{x}_j^H(t + \Delta t_j) e^{j2\pi(f_i \Delta t_i - f_j \Delta t_j)}] = \mathbf{A}_i \mathbf{R}_s^{(ij)} \mathbf{A}_j^H \quad (14)$$

for $i \neq j$, where $\mathbf{R}_s^{(ij)} = I \mathbf{R}_s^{\prime(ij)}$.

Note that, when computing the sample covariance matrices, only T/I data samples are available because the T available samples are equally divided into I frequency components.

B. DOA Estimation

Because the self- and cross-covariance matrices obtained from the frequency-switching sparse arrays have the same form as those of the multi-frequency sparse arrays, the existing methods used for the latter can be similarly exploited. In this paper, we use the group-LASSO approach, described in [20], for this purpose.

The covariance matrices can be vectorized as

$$\mathbf{z}_{ij} = \text{vec}(\mathbf{R}_{ij}) = \tilde{\mathbf{A}}_{ij} \mathbf{b}_{ij} + \sigma_n^2 \mathbf{i}_N \delta(i, j), \quad (15)$$

where $\tilde{\mathbf{A}}_{ij} = [\tilde{\mathbf{a}}_{ij}(\theta_1), \dots, \tilde{\mathbf{a}}_{ij}(\theta_K)]$ such that $\tilde{\mathbf{a}}_{ij}(\theta_k) = \mathbf{a}_i^*(\theta_k) \otimes \mathbf{a}_j(\theta_k)$, $\mathbf{b}_{ij} = \text{vec}(\mathbf{R}_s^{(ij)})$ and $\mathbf{i}_N = \text{vec}(\mathbf{I}_N)$. If the number of grids across the DOA search space is denoted as G , then group-LASSO defines I^2 optimization vectors \mathbf{b}_{ij}^o of size $G \times 1$, and the dictionary matrix on the G -point search grid corresponding to $\tilde{\mathbf{A}}_{ij}$ is denoted as \mathbf{D}_{ij} . The following group sparse optimization problem is formulated:

$$\hat{\mathbf{b}}_{ij}^o = \arg \min_{\mathbf{b}_{ij}^o} \sum_{i=1}^I \sum_{j=1}^I \|\mathbf{z}_{uv} - \mathbf{D}_{ij} \mathbf{b}_{ij}^o\|_2^2 + \zeta \|\mathbf{b}_{ij}^o\|_{1,2}, \quad (16)$$

where ζ denotes the regularization parameter. The DOA estimates across the G search grids are obtained as

$$\hat{\mathbf{b}} = \sum_{i=1}^I \sum_{j=1}^I |\hat{\mathbf{b}}_{ij}^o|. \quad (17)$$

V. NUMERICAL RESULTS

In this section, we provide simulation results that demonstrate the DOA estimation performance of the frequency-switching sparse array which is compared with that of the multi-frequency counterpart. Their CRB results are also compared.

We assume $I = 2$ frequencies applied to a 5-element sparse linear array with physical sensors located at $\mathbb{P} = \{0, 1, 2, 4, 7\}$. The two frequencies are chosen to be mutually coprime as $M_1 = 3$ and $M_2 = 5$. The virtual arrays corresponding to f_1 and f_2 and their union are shown in Fig. 2. Furthermore, an alternate switching pattern with $T = 1,000$ samples over a CPI is considered as shown in Fig. 1. Therefore, for the frequency-switching scheme, each frequency component utilizes $T/2 = 500$ data samples. The input SNR of each frequency component is assumed to be equal and is defined in the frequency-switching case, i.e., all the transmit power is transmitted using a single frequency component. The effective input SNR in the multi-frequency case is divided by a factor of $I = 2$. $K = 10$ targets are uniformly distributed in $[-60^\circ, 60^\circ]$. The grid interval is set to 0.1° and a regularization parameter of $\zeta = 15$ is considered.

Because we only have 9 virtual sensors as shown in Fig. 2, this is an underdetermined DOA estimation problem. It is observed in Figs. 3(a) and 3(b) that, by using the group-Lasso, all the 10 sources are successfully estimated for both frequency-switching and multi-frequency sparse arrays with a similar performance.

To further understand the offerings of the frequency-switching sparse arrays, we compare its CRB with its multi-frequency counterpart. For overdetermined DOA estimation, the CRB is inversely proportional to both the input SNR and the number of snapshots, so the two schemes yield the same CRB [32]. Due to the space limitation, we only compare the CRB for the underlying underdetermined DOA estimation scenario outlined above.

Fig. 4 shows the square-rooted CRB versus the input SNR, and 3 cases are considered, respectively with $T = 500, 5,000$, and $10,000$ data samples. In the low SNR regime, the frequency-switching

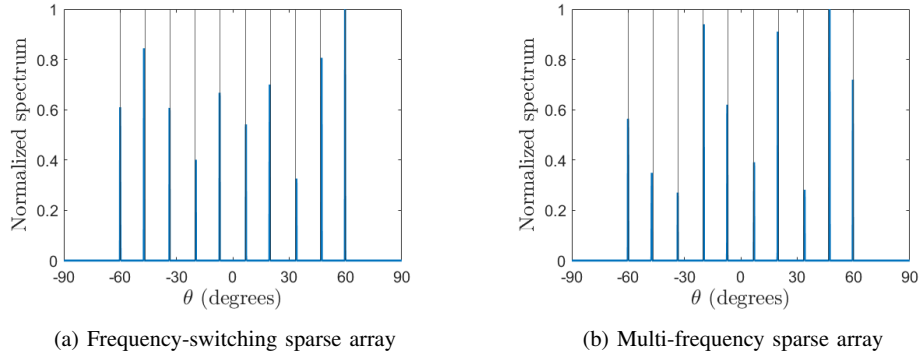


Fig. 3: Group-LASSO spectra of targets using frequency-switching sparse array and multi-frequency sparse array.

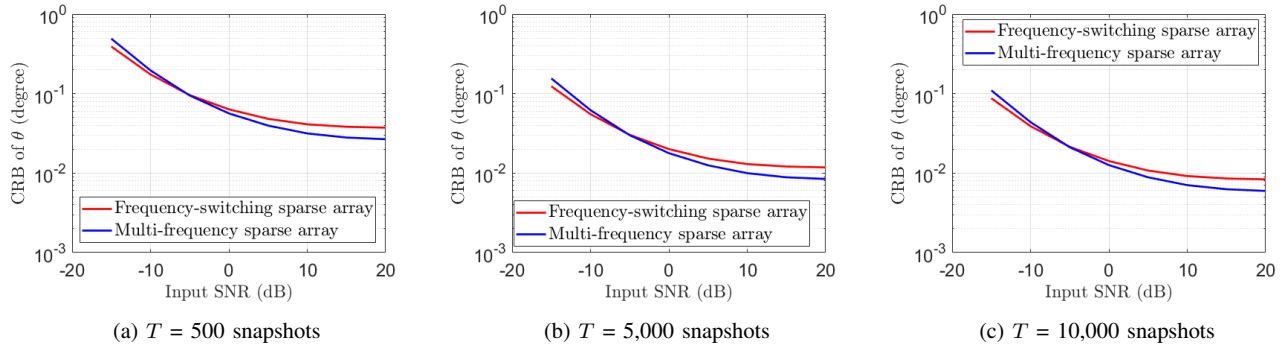


Fig. 4: CRB versus the input SNR for different numbers of snapshots.

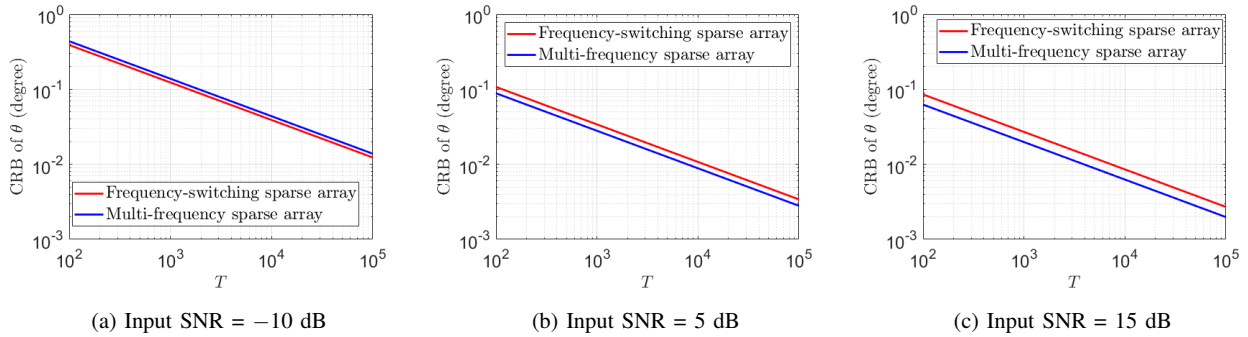


Fig. 5: CRB versus the number of snapshots for different input SNR levels.

sparse array offers a lower CRB because of the higher signal power compared to the multi-frequency counterpart. However, because the CRB has a floor determined by the number of data samples [15, 33], the advantages of the input SNR vanish at the high-SNR regime, and the multi-frequency sparse array is advantageous in this regime because more data samples are used.

In Fig. 5, the CRB results are plotted against the number of snapshots T , where the input SNR is chosen to be -10 dB, 5 dB, and 15 dB. In all cases, the CRB monotonically decreases with T . Regarding the different input SNR cases, as we observed in Fig. 4, the frequency-switching sparse array obtains lower CRB in the low SNR scenario, whereas the multi-frequency sparse array offers a lower CRB when the input SNR is high. Note that the results shown in Figs. 4 and 5 are for the case of $I = 2$, and such differences between the frequency-switching sparse array and the multi-frequency sparse array would become more pronounced as a

higher number of frequencies are used.

VI. CONCLUSION

In this paper, the frequency-switching sparse array scheme was proposed as a low-complexity strategy for the implementation of the multi-frequency sparse arrays. The proposed frequency-switching sparse array achieves the same frequency diversity offered by the multi-frequency counterparts but only requires narrowband data sampling and processing at the receiver. Compared to multi-frequency sparse arrays, a frequency-switching sparse array achieves higher signal power but suffers from reduced number of data samples. For underdetermined DOA estimation, the frequency-switching sparse array achieves a lower CRB than its multi-frequency counterpart at the low-SNR regime, but the multi-frequency sparse array performs better for high input SNR values.

VII. REFERENCES

- [1] A. Moffet, "Minimum-redundancy linear arrays," *IEEE Trans. Antennas Propagat.*, vol. 16, no. 2, pp. 172–175, March 1968.
- [2] R. T. Hoorc and S. A. Kassam, "The unifying role of the co-array in aperture synthesis for coherent and incoherent imaging," *Proc. IEEE*, vol. 78, no. 4, pp. 735–752, April 1990.
- [3] P. P. Vaidyanathan, and P. Pal, "Sparse sensing with co-prime samplers and arrays," *IEEE Trans. Signal Process.*, vol. 59, no. 2, pp. 573–586, Feb. 2011.
- [4] P. Pal and P. P. Vaidyanathan, "Nested arrays: A novel approach to array processing with enhanced degrees of freedom," *IEEE Trans. Signal Process.*, vol. 58, no. 8, pp. 4167–4181, Aug. 2010.
- [5] Z. Zheng, W. Wang, Y. Kong, and Y. D. Zhang, "MISC Array: A new sparse array design achieving increased degrees of freedom and reduced mutual coupling effect," *IEEE Trans. Signal Process.*, vol. 67, no. 7, pp. 1728–1741, April 2019.
- [6] S. Qin, Y. D. Zhang, and M. G. Amin, "Generalized coprime array configurations for direction-of-arrival estimation," *IEEE Trans. Signal Process.*, vol. 63, no. 6, pp. 1377–1390, March 2015.
- [7] C.-L. Liu and P. P. Vaidyanathan, "Super nested arrays: Linear sparse arrays with reduced mutual coupling — Part I: Fundamentals," *IEEE Trans. Signal Process.*, vol. 64, no. 15, pp. 3997–4012, 1 Aug. 2016.
- [8] A. Ahmed, Y. D. Zhang, and B. Himed, "Effective nested array design for fourth-order cumulant-based DOA estimation," in *Proc. IEEE Radar Conf.*, Seattle, WA, May 2017, pp. 998–1002.
- [9] J. Liu, Y. Zhang, Y. Lu, S. Ren, and S. Cao, "Augmented nested arrays with enhanced DOF and reduced mutual coupling," *IEEE Trans. Signal Process.*, vol. 65, no. 21, pp. 5549–5563, Nov. 2017.
- [10] W. Shi, Y. Li, and R. C. de Lamare, "Novel sparse array design based on the maximum inter-element spacing criterion," *IEEE Signal Process. Lett.*, vol. 29, pp. 1754–1758, 2022.
- [11] S. Wandale and K. Ichige, "xMISC: Improved sparse linear array via maximum inter-element spacing concept," *IEEE Signal Process. Lett.*, vol. 30, pp. 1327–1331, 2023.
- [12] X. Li, H. Yang, J. Han, and N. Dong, "A novel low-complexity method for near-field sources based on an S-IMISC array model," *Electronics*, vol. 12, no. 2435, pp. 1–17, 2023.
- [13] X. Sheng, D. Lu, Y. Li, and R. C. de Lamare, "Enhanced MISC-based sparse array with high uDOFs and low mutual coupling," *IEEE Trans. Circuits and Systems II: Express Briefs*, in press.
- [14] Y. D. Zhang, M. G. Amin, F. Ahmad, and B. Himed, "DOA estimation using a sparse uniform linear array with two CW signals of co-prime frequencies," in *Proc. IEEE Int. Workshop Comput. Adv. Multi-Sensor Adaptive Process. (CAMSAP)*, Saint Martin, Dec. 2013, pp. 404–407.
- [15] M. Guo, Y. D. Zhang, and T. Chen, "Performance analysis for uniform linear arrays exploiting two coprime frequencies," *IEEE Signal Process. Lett.*, vol. 25, no. 6, pp. 838–842, June 2018.
- [16] S. Qin, Y. D. Zhang, and M. G. Amin, "DOA estimation exploiting coprime frequencies," in *Proc. SPIE*, vol. 9103, no. 91030E, Baltimore, MD, May 2014, pp. 1–7.
- [17] S. Qin, Y. D. Zhang, M. G. Amin, and B. Himed, "DOA estimation exploiting a uniform linear array with multiple coprime frequencies," *Signal Process.*, vol. 130, pp. 37–46, Jan. 2017.
- [18] Y. Liu and J. R. Buck, "High-resolution direction-of-arrival estimation in SNR and snapshot challenged scenarios using multi-frequency coprime arrays," in *Proc. IEEE Int. Conf. Acoust., Speech Signal Process. (ICASSP)*, New Orleans, LA, March 2017, pp. 3434–3438.
- [19] A. Liu, X. Zhang, Q. Yang, and W. Deng, "Fast DOA estimation algorithms for sparse uniform linear array with multiple integer frequencies," *IEEE Access*, vol. 6, pp. 29952–29965, May 2018.
- [20] A. Ahmed, D. Silage, and Y. D. Zhang, "High-resolution target sensing using multi-frequency sparse array," in *Proc. IEEE Sensor Array Multich. Signal Process. Workshop*, Hangzhou, China, June 2020, pp. 1–5.
- [21] S. Zhang, A. Ahmed, Y. D. Zhang, and S. Sun, "DOA estimation exploiting interpolated multi-frequency sparse array," in *Proc. IEEE Sensor Array Multich. Signal Process. Workshop*, Hangzhou, China, June 2020, pp. 1–5.
- [22] S. Zhang, A. Ahmed, Y. D. Zhang, and S. Sun, "Enhanced DOA estimation exploiting multi-frequency sparse array," *IEEE Trans. Signal Process.*, vol. 69, pp. 5935–5946, Oct. 2021.
- [23] Y. D. Zhang and M. G. Amin, "Multi-frequency rational sparse array for direction-of-arrival estimation," in *Proc. Int. Symp. Signals, Circuits and Systems*, Iași, Romania, July 2023, pp. 1–4.
- [24] M. W. T. S. Chowdhury and Y. D. Zhang, "Unambiguous DOA estimation using multi-frequency rational sparse arrays," in *Proc. Asilomar Conf. Signals, Systems, Computers*, Pacific Grove, CA, Oct. 2023.
- [25] R. O. Schmidt, "Multiple emitter location and signal parameter estimation," *IEEE Trans. Antennas Propagat.*, vol. 34, no. 3, pp. 276–280, March 1986.
- [26] L. Meier, S. V. D. Geer, and P. Buhlmann, "The group lasso for logistic regression," *J. R. Statist. Soc. B*, vol. 70, no. 1, pp. 53–71, Feb. 2008.
- [27] N. Simon and R. Tibshirani, "Standardization and the group lasso penalty," *Stat. Sin.*, vol. 22, no. 3, pp. 983–1001, June 2012.
- [28] S. Sun and Y. D. Zhang, "4D automotive radar sensing for autonomous vehicles: A sparsity-oriented approach," *IEEE J. Sel. Topics Signal Process.*, vol. 15, no. 4, pp. 879–891, June 2021.
- [29] L. Xu, S. Sun, K. V. Mishra, and Y. D. Zhang, "Automotive FMCW radar with difference co-chirps," *IEEE Trans. Aerosp. Electron. Syst.*, vol. 59, no. 6, pp. 8145–8165, Dec. 2023.
- [30] Y. D. Zhang and S. Sun, "Identical partitioning of consecutive integer set," in *Proc. IEEE Sensor Array and Multich. Signal Process. Workshop*, Corvallis, OR, July 2024.
- [31] D. H. Johnson and D. Dudgeon, *Array Signal Processing*. Prentice Hall, 1993.
- [32] P. Stoica and A. Nehorai, "MUSIC, maximum likelihood, and Cramer-Rao bound," *IEEE Trans. Acoust., Speech, Signal Process.*, vol. 37, no. 5, pp. 720–741, May 1989.
- [33] C.-L. Liu and P. P. Vaidyanathan, "Cramér-Rao bounds for coprime and other sparse arrays, which find more sources than sensors," *Digital Signal Process.*, vol. 61, pp. 43–61, Feb. 2017.